SRTTU

JCARME
ISSN: 2228-7922
Journal of Computational and Applied Research in Mechanical Engineering
Vol. 9, No. 2, pp. 211-223
jcarme.sru.ac.ir

Numerical analysis of heat transfer enhancement and flow structure of alternating oval tubes by considering different alternate angles under turbulent flow

Hasan Najafi Khaboshan and Hamid Reza Nazif *

Department of Mechanical Engineering, Imam Khomeini International University, Qazvin, Iran

Article info:
Type: Research
Received: 09/10/2017
Revised: 22/10/2018
Accepted: 24/10/2018
Online: 27/10/2018

Keywords:
Turbulent flow,
Heat transfer,
Friction factor,
Nusselt number,
Multi-longitudinal vortex,
Alternating oval tube.

Abstract

In this research, the convective heat transfers of turbulent water fluid flow in alternating oval tubes is studied using computational fluid dynamics. The purpose of the study is to analyze the heat transfer enhancement and secondary internal flows under different alternate angles. Also, comparing the effect of two schemes for the domain discretization to be used in the solution variables' gradients on simulation results is investigated. The secondary flow causes an increase in the numbers of multi-longitudinal vortices (MLV) by changing the angle of pitches. These phenomena permit the cold fluid flow to stream in more paths from center to tube wall and better condition for mixing of fluids. Consequently, the heat transfer enhances by using the alternating oval tubes. However, forming the multi-longitudinal vortices causes an increase in pressure drop. Also, by raising the angle of pitches, the friction factor and the average of Nusselt number are amplified. It is also observed that the average heat transfer coefficient in the transition range is more than other areas. The mean Nussult numbers of this kind of tubes in the angles of 40°, 60°, 80°, and 90° improved 7.77%, 14.6%, 16.93%, and 24.42%, respectively in comparison with the round tube. The performance evaluation criteria (*PEC*) for all alternating oval tubes under the constant inlet velocity boundary condition indicated that the highest value (*PEC*=1.09) had been obtained at the lowest Reynolds number (*Re*=10,000) in the alternating oval tube 90°.

Nomenclature

A	Area, m^2
C_p	Specific heat, J kg^{-1} K^{-1}
D_h	Hydraulic diameter, m
f	Friction factor, $f = (\Delta p\, D_h)/(\frac{1}{2}\, \rho\, u_{avg}^2\, L)$
g	Gravitational acceleration, m s^{-2}
h	Heat transfer coefficient, W m^{-2} K^{-1}
K	Thermal conductivity, W m^{-1} K^{-1}
k	Turbulent kinetic energy, m^2 s^{-2}
L	Total length of the tube, mm
Nu	Nusselt number, $Nu = (q^{''} D_h)/(K\,(T_w - T_b))$
P	Pressure, kg m^{-1} s^{-2}
P	Pitch length, mm
$\overline{P}$	Mean pressure, kg m^{-1} s^{-2}
P_k	Generation of k, kg m^{-1} s^{-3}
Pr	Prandtl number, $Pr = \mu\, C_p/K$
$q^{''}$	Heat flux, W m^{-2}
Re	Reynolds number, $Re = \rho\, u\, D_h/\mu$
T	Temperature, K
T_b	Average of bulk temperature, K
$\overline{T}$	Mean temperature, K
T'	Turbulent temperature fluctuations, K

*Corresponding author
email address: nazif@eng.ikiu.ac.ir

u_i	Velocity, m s^{-1}
$\overline{u_i}$	Mean velocity, m s^{-1}
u_i'	Turbulent velocity fluctuations, m s^{-1}
x_i	Cartesian coordinates, m
y^+	Non-dimensional wall distance, $y^+ = (\sqrt{\tau_w/\rho}\ Y)/\upsilon$
Y	Closest distance from the wall, m
z	Axial distance from the inlet, m

Greek symbols

δ_{ij}	Kronecker delta
ε	Turbulent dissipation rate, $m^2\ s^{-3}$
μ	Laminar dynamic viscosity, kg $m^{-1}\ s^{-1}$
μ_t	Turbulent dynamic viscosity, kg $m^{-1}\ s^{-1}$
υ	Kinematic viscosity, $m^2\ s^{-1}$
ρ	Density, kg m^{-3}
σ_k	Turbulent Prandtl number of k
σ_ε	Turbulent Prandtl number of ε
τ_{ij}	Stress tensor,s kg $m^{-1}\ s^{-2}$

Subscripts

avg	Average
eff	Effective
s	Base tube
w	Wall

1. Introduction

Improving the heat transfer in different heat exchangers is very important for industrial applications, like petroleum industry, vehicle industry, chemical engineering, etc.

Several techniques in the improvement of heat transfer are presented to increase the heat transfer of heating devices such as reducing pressure loss and boosting the performance by optimizing heat transfer rate. For instance, changing the geometry of the tubes of the heat exchanger for improving the heat transfer is one of those techniques [1].

Meng et al. [2] investigated the alternating oval (AO) tubes with water as the working fluid experimentally. They analyzed convective heat transfer within a wide range $500 < Re < 5\times10^4$. Furthermore, they observed that the heat transfer of the alternating oval tubes is more than that of the twisted elliptical and the corrugated tubes for equal pumping power. Their analysis revealed that the multi-longitudinal vortices (MLV), created by changing the cross-section in the AO tubes, improved the heat transfer.

Sajadi et al. [3] analyzed flow resistance and heat transfer of oil flow in a circular, flattened and AO tubes, numerically and empirically. Their simulation outcomes illustrated that increasing the pitch length and aspect ratio increased flow resistance and heat transfer. In addition, they realized that AO tubes performed better than circular or flattened tubes.

The rate of heat transfer increased by creating the MLV in the turbulent flow of the AO tube. Considering the latest studies [4-6], all analyses were only done within AO tube with the angle of 90°. So, in this research, the forced convection heat transfer of turbulent flow in AO tubes is investigated numerically in various alternating angles. First, the least squares cell-based (LSCB) and the green gauss node-based (GGNB) schemes were compared with each other for the domain discretization of gradients of the solution variables in numerical analysis. Then, some factors of the convective turbulent flow were compared with the AO tube under different alternative angles. In the end, for studying the overall thermo-hydraulic performance of the AO tubes, the average Nusselt number (Nu_{avg}), friction factor (f) and the performance evaluation criterion (PEC) for the same given pump power were investigated.

2. Mathematical model

2.1. Geometry of model

The alternating oval tube can be applied to improve heat transfer [7]. The AO tube consists of alternate sections whose cross-section is oval and their axes have 40°, 60°, 80°, and 90° rotation between each other for each tube. Between these alternate parts, the transition sections are linked with them. Fig. 1 illustrations the geometrical construction of the AO tube for all angles used in the current study. In addition, the inlet and outlet of the AO tube have a round cross-section with a diameter of d and length of L_d. According to Fig. 1, the parameter of C represents the length of the transition section, P is the length of pitches, θ shows the angle between the main axes of the oval section, and parameters of A and B signify the main and secondary axes measurements of the oval section, respectively. Table 1 shows the value of these parameters for the AO tubes. In this table, the parameters of N and L defined the numbers

of alternating oval section and the full length of the AO tubes, respectively.

2.2 Theoretical formulation

In the current study, the numerical analysis of the convective turbulent flow was implemented by the FV method. The Reynolds-averaged Navier Stokes (RANS) equations were intended for numerical computation. The continuity, momentum, and energy equations of the turbulence are considered as follows, respectively [8]:
Continuity equation:

$$\frac{\partial \overline{u}_i}{\partial x_i}=0 \tag{1}$$

Momentum equation:

$$\rho\overline{u}_j\frac{\partial \overline{u}_i}{\partial x_j}=-\frac{\partial \overline{P}}{\partial x_i}+\frac{\partial}{\partial x_j}\left(\mu\frac{\partial \overline{u}_i}{\partial x_j}-\rho\overline{u_i'u_j'}\right) \tag{2}$$

Energy equation:

$$\rho C_p\overline{u}_i\frac{\partial \overline{T}}{\partial x_i}=\frac{\partial}{\partial x_j}\left(K\frac{\partial \overline{T}}{\partial x_j}-\rho C_p\overline{u_i'T'}+\overline{u}_i\left(\tau_{ij}\right)_{eff}\right) \tag{3}$$

It should be noted that the viscous dissipation term is considered at the end of the energy equation which is written as follows:

$$\left(\tau_{ij}\right)_{eff}=\mu_{eff}\left(\frac{\partial \overline{u}_j}{\partial x_i}+\frac{\partial \overline{u}_i}{\partial x_j}\right)-\frac{2}{3}\mu_{eff}\frac{\partial \overline{u}_k}{\partial x_k}\delta_{ij} \tag{4}$$

The standard k-ε equations were used for modeling turbulent flow. The formulations of two turbulent parameters (k and ε) were calculated from the following formulations [9]:

$$\frac{\partial}{\partial x_i}(\rho k\overline{u}_i)=\frac{\partial}{\partial x_j}\left[\left(\mu+\frac{\mu_t}{\sigma_k}\right)\frac{\partial k}{\partial x_j}\right]+P_k-\rho\varepsilon \tag{5}$$

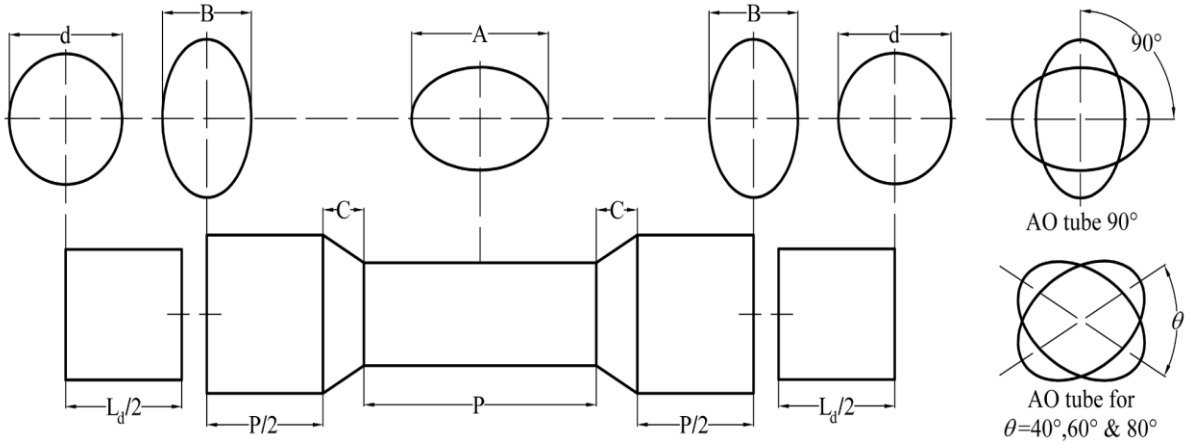

Fig. 1. Construction of the alternating oval tubes in the present study.

Table 1. The value of geometrical parameters of the AO tubes.

A (mm)	B (mm)	P (mm)	C (mm)	d (mm)	L_d (mm)	N	L (mm)
20	13	34	6	16.5	34	11	514

$$\frac{\partial}{\partial x_i}(\rho\varepsilon\overline{u_i}) = \frac{\partial}{\partial x_j}\left[\left(\mu+\frac{\mu_t}{\sigma_\varepsilon}\right)\frac{\partial\varepsilon}{\partial x_j}\right] + C_{1\varepsilon}\frac{\varepsilon}{k}P_k - \rho C_{2\varepsilon}\frac{\varepsilon^2}{k} \quad (6)$$

where μ_t represents the dynamic viscosity of turbulent, and P_k is the generation of turbulent kinetic energy defined as:

$$\mu_t = \rho C_\mu \frac{k^2}{\varepsilon} \quad (7)$$

$$P_k = -\rho\overline{u_i'u_j'}\frac{\partial\overline{u}_j}{\partial x_i} \quad (8)$$

The model constants have the following values [9]:

$C_{1\varepsilon}$=1.44, $C_{2\varepsilon}$=1.92, C_μ=0.09, σ_k=1 and σ_ε=1.3

For modeling the manner of fluid flow near the tube wall, the enhanced wall treatment method was used. Two length scales (ℓ_μ and ℓ_ε) in this model are defined as the turbulent viscosity (μ_t) and dissipation rate (ε) near the wall domain, which turbulent kinetic energy has been already calculated [10]:

$$\mu_t = \rho C_\mu \ell_\mu \sqrt{k} \quad \text{and} \quad \varepsilon = \frac{k^{3/2}}{\ell_\varepsilon} \quad (9)$$

where

$$\ell_\mu = yC_l^*\left(1-\exp(-Re_y/A_\mu)\right) \quad (10)$$

$$\ell_\varepsilon = yC_l^*\left(1-\exp(-Re_y/A_\varepsilon)\right) \quad (11)$$

$$Re_y = \frac{\rho y\sqrt{k}}{\mu} \quad (12)$$

The constants values of Wolfshtein model [11] were considered as follows:

C_μ=0.09, $C_l^*=\kappa\, C_\mu^{3/4}$, A_μ=70, $A_\varepsilon=2C_l^*$ and κ= 0.4187

In addition, one of the serious limitations in this study was mesh generation strategy for enhanced wall treatment method. For low Reynolds number boundary layer, the aspect ratio and skewness of grids near the wall should be justified as the cross-section is rotated. To overcome this drawback, the finer mesh is used in the transition zones.

2.3 Explanation of boundary conditions

The velocity inlet and outflow boundary conditions were considered for the input and output of the circular cross-section of all tubes, respectively. The uniform velocity profile, which had been considered normal to the boundary, was defined for the inlet boundary condition of the AO tubes. In all numerical computations, the inlet velocity was calculated from the input Reynolds number and the inlet temperature was constant that was equal to 295 Kelvin, according to Ref. [12]. The no-slip boundary condition situation was applied on the wall of the tube. In addition, the wall temperature boundary condition was constant and it was equal to 325 Kelvin.

3. Numerical solution

Numerical results of the forced convection heat transfer of turbulent flow had been calculated by applying the FV method. The SIMPLEC algorithm was applied for the pressure-velocity coupling of equations [13, 14]. The gradients of the solution variables in cell centers of elements for the turbulence and energy discretization were set by the LSCB [15] and the GGNB [16, 17] schemes, respectively. Therefore, the RANS and turbulence formulations were initially solved. Afterward, the energy parameters were calculated, while all variables of flow were freezing. In calculating the pressure of cell-faces, the standard scheme [15] was used. Also, to discretize all equations, the second order upwind [18] scheme was applied. Beside, to capture the phenomena of boundary layer near the tube wall, the enhanced wall treatment method [19] was used. In this method, the dimensionless factor of y^+ for the initial cell center from the tube wall was near to or smaller than one. The variables had been stored with the double precision. Also, the calculation of all solution variables continued until the residuals of parameters for all equations were lower than 10^{-6}.

3.1 Grid independence study

To select a suitable grid number for numerical simulations, five different grids had been compared with each other for the AO and circular tubes (base tube). Fig. 2 illustrates the mesh layout of the AO tube 90°, 60°, and the base tube which has been used in the current numerical simulations. The number of elements of five different meshes for the AO tube 90° are shown in Table 2. In this Table, the value of the Nu_{avg} had been calculated for the AO tube 90° at Re=40,000 under the boundary conditions cited in part 2.3. The friction factor of turbulence and the average of the Nusselt number were calculated from the following equations:

$$f = \frac{\Delta p \, D_h}{\frac{1}{2}\rho u_{avg}^2 \, L} \tag{13}$$

$$Nu_{avg} = \frac{1}{L}\int_0^L \frac{q''_{avg} \, D_h}{K\,(T_w(z) - T_b(z))}\, dz \tag{14}$$

where Δp and $T_b(z)$ represent the difference in total pressure along the tube, and the average of bulk temperature, respectively.

$$T_b(z) = \frac{1}{A u_{avg}} \int_A uT \, dA \tag{15}$$

Table 2. Variations of the average Nusselt number versus the number of elements.

Mesh (number of elements)	Nu_{avg}	δNu
Mesh-one (1,444,608)	280.9442	-
Mesh-two (1,932,800)	339.2751	-58.3309
Mesh-three (3,379,376)	343.5931	-4.318
Mesh-four (3,951,360)	345.0233	-1.4302
Mesh-five (4,646,340)	346.0065	-0.9832

As mentioned before, to select a suitable grid number, the numbers of five different meshes were compared. From Table 2, it can be found that the relative deviation of the Nu_{avg} for the mesh-four is smaller than previous meshes

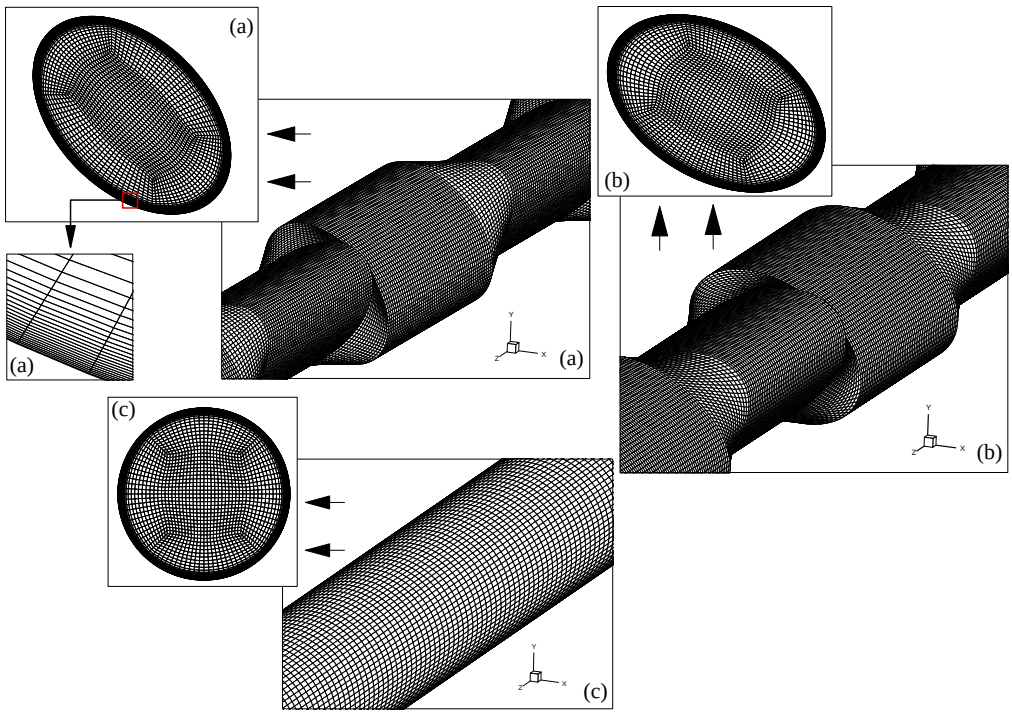

Fig. 2. Mesh domain of the AO tubes for various angles of pitches (a) θ=90°, (b) θ=60° and (c) the circular ones.

(mesh one to three). So, the element numbers of the mesh-four are independent and appropriate for all numerical simulations.

3.2 Numerical results validation of the AO tube

To study the precision of the simulation, the numerical results of this research should be investigated with empirical results. The force convection heat transfer within the AO tube 90° was studied by Guo [12] in 2003 under the turbulent flow regime. In the current research, the parameters of the AO tube 90° are similar to his study. Fig. 3 shows the comparison between the numerical results of this research with the experimental data of Guo [12] and the numerical results of Chen et al. [20] for an AO tube 90°. In this figure, water is the working fluid and *Re* varies from 10,000 to 60,000. As illustrated in Fig. 3, the numerical results of this study are in passable contrast with empirical data which was reported by Guo [12]. Furthermore, the simulation results of this research are more appropriate than the simulation results of Ref. [20]. The largest absolute deviations between the experimental and numerical data of the f and Nu_{avg} in the AO tube 90° have been detected around 14% and 6.5%, respectively. On the other hand, all these values for the AO tubes 90° are smaller than the previous numerical results, which were presented by Sajadi et al. [3] (for the f and Nu_{avg} are about 21% and 24%, respectively). Afterwards, it can be determined that the numerical model of this research is appropriate for simulating the forced convection heat transfer of turbulent flow within the AO tubes.

As displayed in Fig. 3(a), by applying the LSCB scheme instead of the GGNB scheme for the gradients of the solution variables, the simulation results of the f are improved. Also, the numerical results of the Nu_{avg} using the GGNB scheme present good agreement with experimental results compared with the LSCB scheme (See Fig. 3(b)). From these numerical results, the LSCB and GGNB schemes are appropriate to discretize the turbulence and thermal equations, respectively.

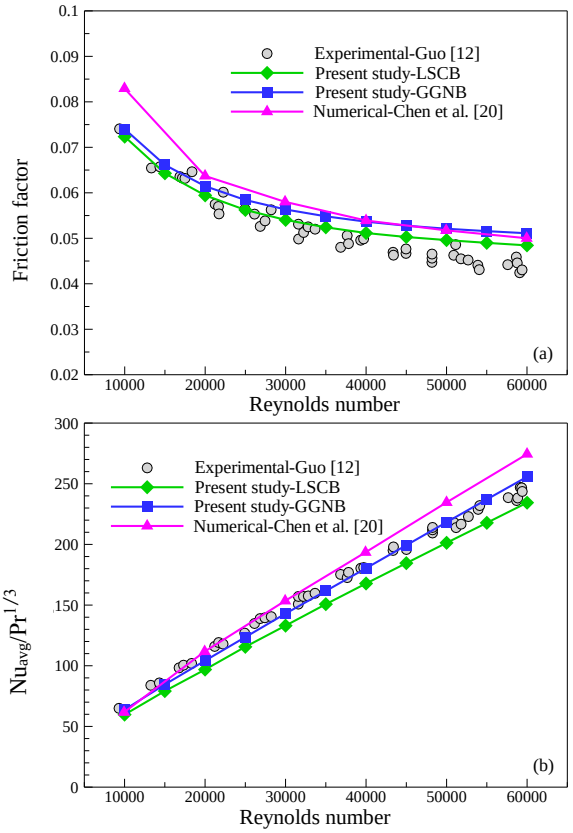

Fig. 3. Comparison of the (a) f and (b) $Nu_{avg}/Pr^{1/3}$ with existing empirical [12] and simulation [20] data of AO tube 90°.

3.3 Numerical results validation of the base tube

To compare the numerical results of the AO tubes with the circular tube, we must also simulate a circular tube. The friction factor correlation in fully developed flow for the round smooth surface tubes in the range of $3{,}000 \lesssim Re \lesssim 5\times10^6$ has been developed by Petukhov et al. [21]. Also, for the Nusselt number, there is an experimental correlation in the fully developed flow and the validity for the round tubes is provided by Gnielinski [22, 23]. This correlation is valid for $3{,}000 \lesssim Re \lesssim 5\times10^6$ and $0.5 \lesssim Pr \lesssim 2{,}000$. The two correlations were calculated as follows:

$$f_s = (0.79\ln(Re) - 1.64)^{-2} \tag{16}$$

$$Nu_s = \frac{(f/8)\,(Re - 1000)\,Pr}{1 + 12.7(f/8)^{1/2}\left(Pr^{2/3} - 1\right)} \tag{17}$$

Fig. 4 demonstrates the evaluation between the f and Nu_{avg} for the round tube after a fully developed flow with both correlations mentioned in the previous paragraph. As is evident from Fig. 4, there is good agreement between the current simulation results and the empirical associations (Eqs. (16 and 17)).

4. Results and discussion

In the present part of the research, the hydrodynamic parameters of the convective turbulent flow are investigated in alternating oval tubes. Therefore, quantities such as the velocity vector, the static pressure, temperature, and the *PEC* are discussed in detail.
Some results were calculated in cross-sections which were called distance A, and B (See Fig. 5). According to this figure, this section of AO tube had been placed among 0.357 to 0.437 m from the input of tube. Between these sections, there is a distance called the transition length, which is briefly illustrated in the figure as a transition. In this region (transition length), three cross-sections had been chosen to exhibit some numerical results. Sections A and B had been located at the entrance and exit of the transition region, respectively. Section C was positioned next to the transition region (in the half of the distance B).

4.1 Flow structures

To review the flow structure within each of AO tube affected by changing the angle θ, the streamlines and the contour of the static pressure in three Sections A, B, and C in Fig. 6 are investigated. As can be observed, on two sides of the main diameter of Sections A and B, the amount of pressure is maximum. Given that Section B is rotated with respect to Section A, this causes the MLV in the flow. Also, turbulence-driven secondary motions can develop the MLV in such non-circular ducts. By alternating the cross-section with primary section, the MLV are generated resulting more circulation in fluid flow along the tube wall consequently permits more heat transfer to the walls. In addition, the MLV has been extended by increasing the difference of

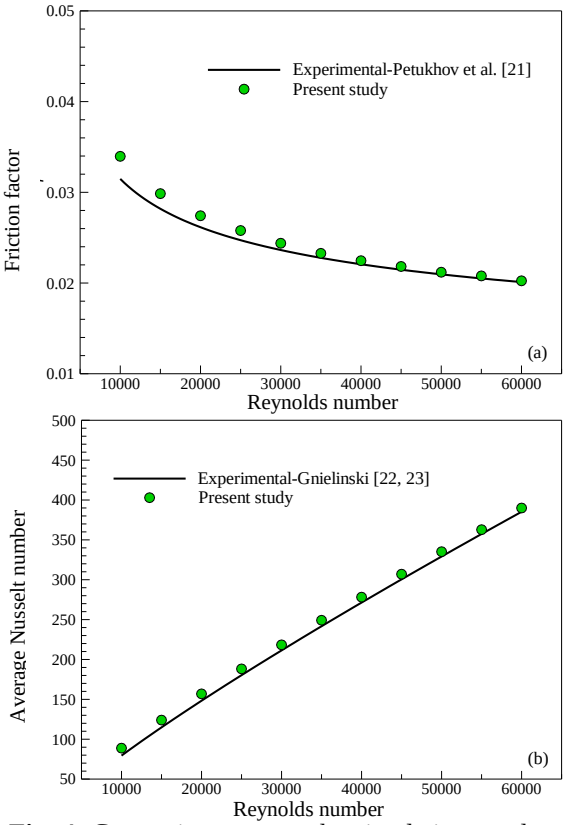

Fig. 4. Comparison among the simulation results of (a) the f and (b) Nu_{avg} with the empirical correlation of Petukhov et al. [21] and Gnielinski [22, 23] for a round tube.

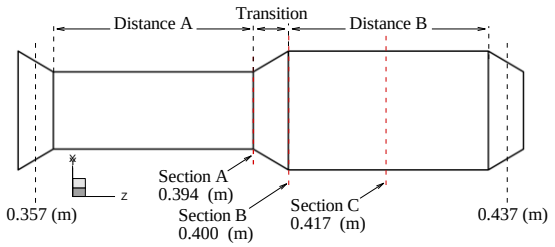

Fig. 5. The range of analysis for some results and the positions of three different sections.

the pressure between two Sections A and B, and increasing the angle of θ. The secondary flows have been generated in Section B and are marked with red dash lines in Fig. 6. It is observed that only in two AO tubes 80° and 90°, the secondary flows have been generated in Section B. This can be explained by the creation of two high-pressure zones at the end of the main diagonal of Section B. Then, by moving away from the transition zone, the secondary flows devote a wider zone of

the cross-section area of Section C to themselves. From Section C of the AO tubes 40° and 60°, it is obvious that four vortices in the cross-section of tubes have been generated, but in two other tubes, the number of vortices is eight. These results indicate that the number of MLV increases with increasing the angle of θ. It is also observed that the pressure change in the cross-section of the two Sections A and B is more than in Section C, which shows that the pressure difference in the tube cross-section is due to the geometry change along the tube.

Therefore, the rising of the pressure losses results from the existence of the MLV, which has been generated within the AO tubes.

4.2 Distribution of heat transfer

To investigate the changes of temperature field under the influence of MLV in the AO tubes, the vectors of velocity and the temperature contour are illustrated at Section C of the four tubes in Fig. 7. This figure shows that cold fluids located at the tube center move toward the wall of the AO tubes along with some paths which are marked in Fig. 7.

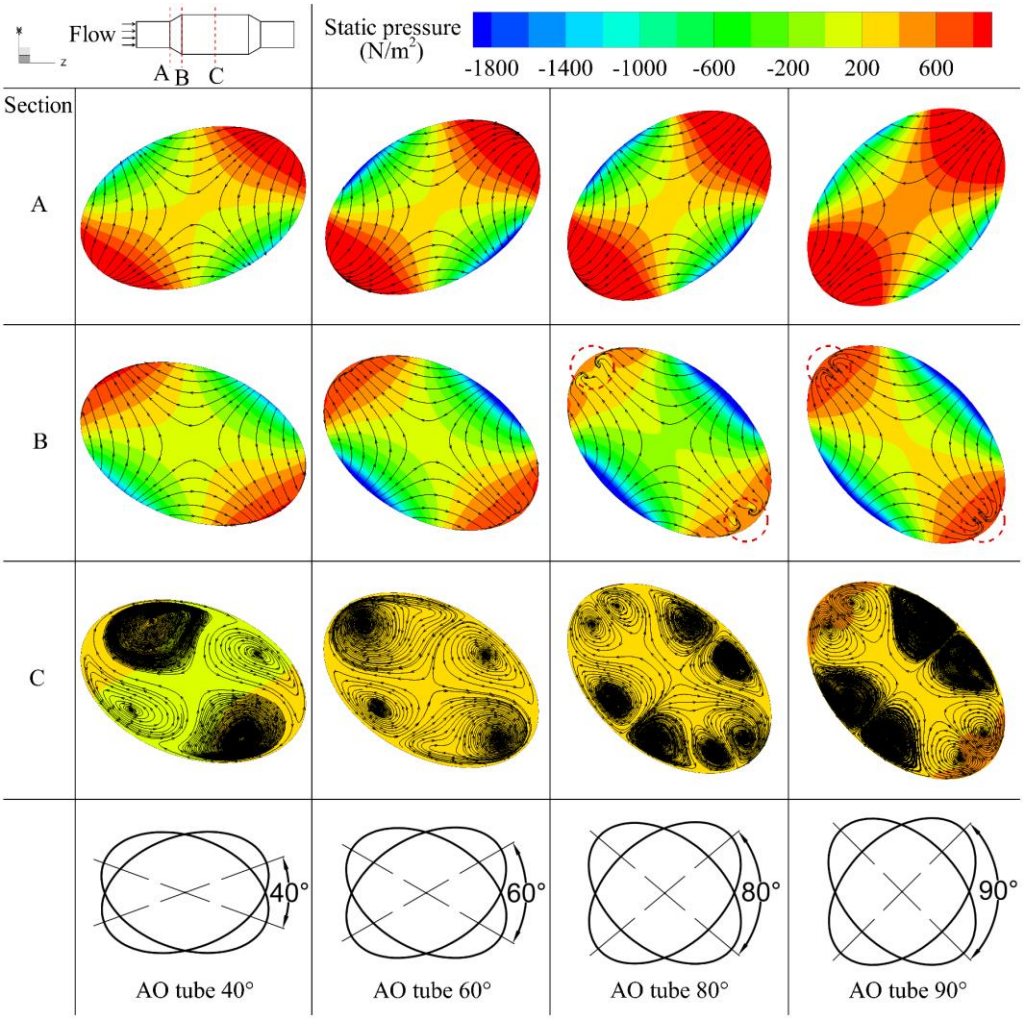

Fig. 6. Streamline and static pressure in the three cross-sections of the AO tubes per various θ (*Re*=40,000).

Those paths were created by moving the secondary flow. After that, the cooling water fluids are combined with the warmed fluids near the wall of the tube. Then, due to the motion of secondary flows, the heated fluids are transmitted towards the center of the tube section. This kind of fluids movement in the turbulent flow comes from the existence of the MLV inside the tube. This phenomenon makes the high-temperature, the great gradient of temperature, and the slim boundary layer adjacent to the tube wall which leads to improving the heat transfer performance.

From investigating the contour of the temperature and the vector of velocity in these AO tubes, it was evident that the field of temperature has been affected by MLV. Also, with enhancing the angle of θ, the numbers of MLV have been augmented. It causes the mass flow rate of the cooling fluid from the center of the tube toward the hot fluid to increase. In addition, the cold and hot water are better combined when the numbers of the MLV increase.

The average of heat transfer coefficient (h_{avg}) along the specific length of the AO tubes is illustrated in Fig. 8. It can be found that the values of h_{avg} at transition zones are higher than others, and their values have been reduced after some distances from the transition section. These behaviors due to the good collision between cold and hot fluids are concluded by the MLV. From one side, it can be found that because of increasing the number of MLV, the value of heat transfer increases as the angle of θ increase. In this research, the average of heat transfer coefficient has been computed as follows:

$$h_{avg} = \frac{q''_{avg}}{(T_w - T_b)} \tag{18}$$

where, q''_{avg} represents the mean of heat flux around the AO of the wall of the tube.

4.3 Analysis of friction factor and Nusselt number

The turbulent friction factor and the average of the Nusselt number were calculated for studying the thermal-hydraulic performance of the AO tubes and circular ones under the various angle of θ. The effect of raising the *Re* on both of these parameters has been investigated in Fig. 9 (a) and (b), respectively. As has been displayed, with increasing the Reynolds number the *f* has been reduced in all tubes. Furthermore, the value of the *f* for the AO tube 40° is more than the base tube. According to Fig. 9 (b), the Nu_{avg} has been enhanced with raising the *Re*. In addition, as compared to the base tube, the value of the Nu_{avg} for the AO tube 40° is more.

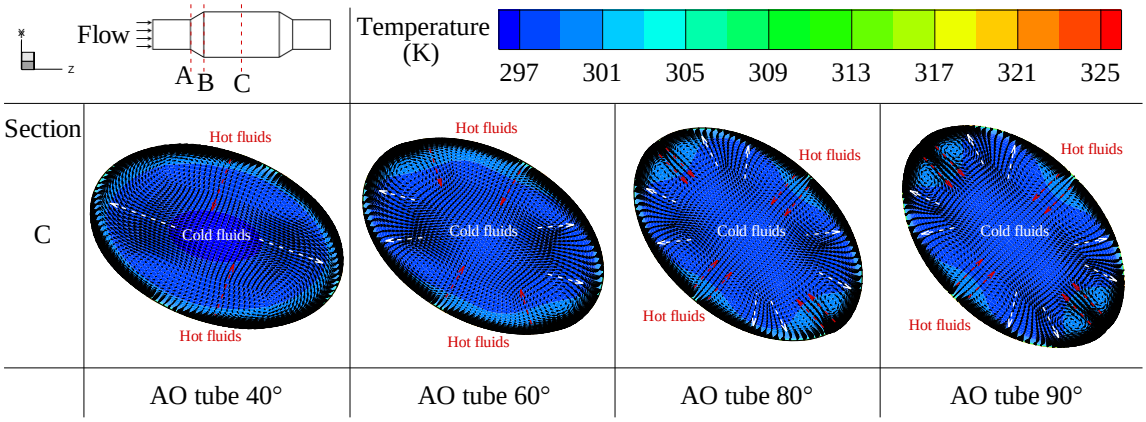

Fig. 7. The temperature contour and the vector of velocity on Section C of the AO tubes per various θ (*Re*=40,000).

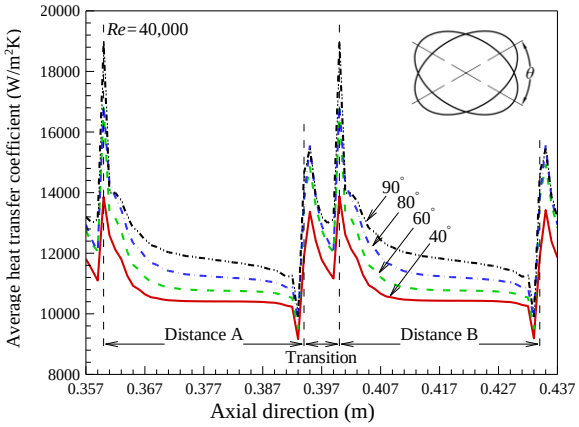

Fig. 8. Variations of the average heat transfer coefficient of the AO tubes per various θ (*Re*=40,000).

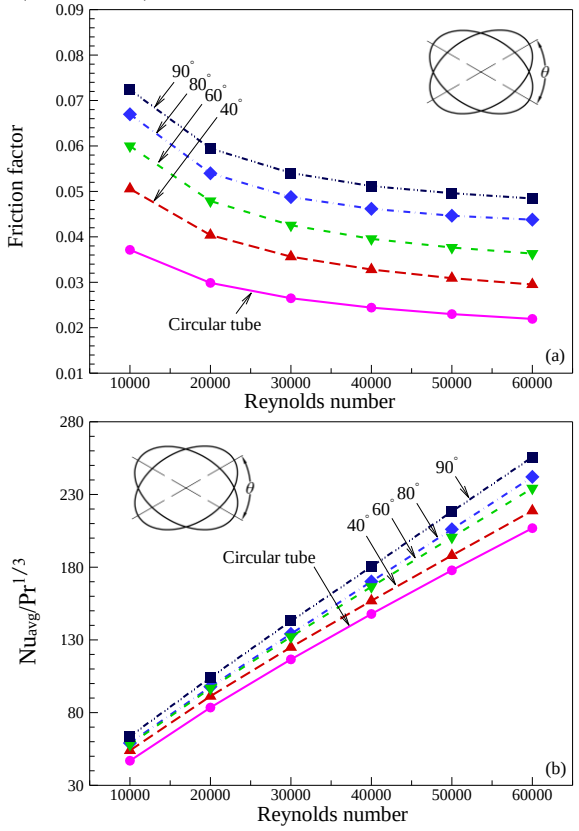

Fig. 9. Variations of (a) the f and (b) the Nu_{avg} with increasing the *Re* for tubes which have been considered in current research.

Also, both parameters have increased as the angle of θ increases. This is due to an increase in numbers of the MLV inside the fluid flow. The enhancement of the mean Nussult numbers for the AO tubes in the angles of 40°, 60°, 80°, and 90° are around 7.77%, 14.6%, 16.93%, and 24.42% compared with the base tube, respectively. As previously mentioned, the heat transfer of the AO tube 90° is more than the other tubes, but this advantage has the highest pressure drop.

4.4 Investigation of the PEC

To have useful numerical results of the convective turbulent flow in the AO tubes, the *PEC* has been presented by Webb and Kim [24] to assess the performance of thermal-hydraulic of the improved tubes at the same power of pumping. The *PEC* had been computed as follows:

$$PEC = \frac{Nu/Nu_s}{(f/f_s)^{1/3}} \tag{19}$$

where Nu_s and f_s are the Nusselt number and friction factor of the base tube, respectively.
The variation of the *PEC* with increasing the Reynolds number has been illustrated in Fig. 10 for all AO tubes. As shown in this figure, from Reynolds number of 20,000 to over, the value of *PEC* is smaller than number 1. Also, the maximum amount of *PEC* for every AO tube has been achieved at a small *Re*. In Reynolds number of 10,000, it is observed that the *PEC* has increased with increasing the angle of θ (except for the AO tube 80°). The maximum *PEC*, which is equal to 1.09, is achieved in the AO tube 90° for the least *Re*. Therefore, this value of the *PEC* demonstrates that the AO tubes are more efficient than the base tube. Finally, it could be reached to the fact that furthering the numbers of MLV with increasing the angle of θ enhances the heat transfer as compared to smaller values of angle θ.

5. Conclusions

In this research, the convective heat transfer and flow structure of the alternating oval tubes were numerically studied under different alternative angles. All the numerical simulations were calculated in the Reynolds numbers of

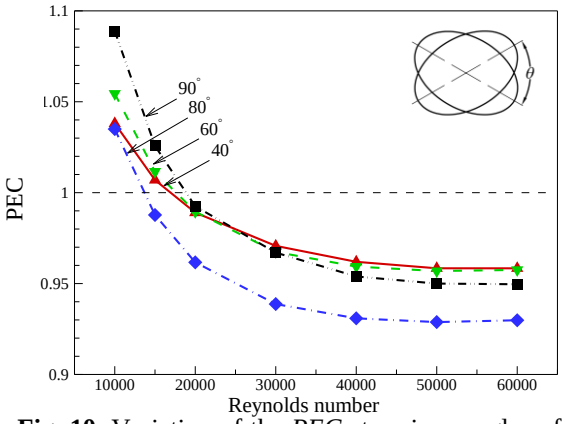

Fig. 10. Variation of the *PEC* at various angles of θ for all AO tubes.

10,000-60,000. The simulation results of this research had a reasonable conformity with available experimental data by using the standard k-ε turbulence model. The calculation of the f and Nu_{avg} with the LCCB and GGNB schemes respectively for the domain discretization to be used in the gradients of the solution variables had the least relative deviation with the empirical data.

By examining the streamlines, it was observed that the initial of secondary flows were seen in the output section of the transition zone. By following the fluid along the tube, the secondary flows, according to what was observed from the cross-sections of the tube, become larger. Also, the MLV was broken along the constant cross-section of AO tubes, by increasing the angle of θ from 60° to 80°, whose numbers increased from 4 to 8.

The existence of the MLV inside the turbulent flow and increasing their numbers as increased the angle θ, caused the hot and cold fluids to be combined together well and improve the rate of heat transfer.

The numerical results showed that the heat transfer of AO tubes was more than the base tube. Moreover, the value of the f and Nu_{avg} reduced and enlarged, respectively, with increasing the *Re*. Also, by increasing the angles of θ. both of these parameters had increased.

In addition, the maximum value of the *PEC* (1.09) was obtained at the lowest Reynolds number for the AO tube 90°. It was also seen that the value of *PEC* was less than one in $Re \geq$ 20,000, indicating that the utility of the AO tube in this range of *Re* is less economical in comparison to the base tube.

As the aim of this research is studying the flow structure and improvement of the heat transfer performance, the future research tends to capture and analyze other types of thermal boundary conditions along the wall of the tube by using nanofluids instead of pure water fluid.

References

[1] H. Najafi Khaboshan, and H. R. Nazif, "Investigation of heat transfer and pressure drop of turbulent flow in tubes with successive alternating wall deformation under constant wall temperature boundary conditions", *Journal of the Brazilian Society of Mechanical Sciences and Engineering*, Vol. 40, No. 2, p. 42, (2018).

[2] J.-A. Meng, X.-G. Liang, Z.-J. Chen, and Z.-X. Li, "Experimental study on convective heat transfer in alternating elliptical axis tubes", *Experimental Thermal and Fluid Science*, Vol. 29, No. 4, pp. 457-465, (2005).

[3] A. R. Sajadi, S. Yamani Douzi Sorkhabi, D. Ashtiani, and F. Kowsari, "Experimental and numerical study on heat transfer and flow resistance of oil flow in alternating elliptical axis tubes", *International Journal of Heat and Mass Transfer*, Vol. 77, pp. 124-130, (2014).

[4] W.-L. Chen, and W.-C. Dung, "Numerical study on heat transfer characteristics of double tube heat exchangers with alternating horizontal or vertical oval cross section pipes as inner tubes", *Energy Conversion and Management*, Vol. 49, No. 6, pp. 1574-1583, (2008).

[5] J.-A. Zambaux, J.-L. Harion, S. Russeil, and P. Bouvier, "The effect of successive alternating wall deformation on the performance of an annular heat exchanger", *Applied Thermal Engineering*, Vol. 90, pp. 286-295, (2015).

[6] H. Najafi Khaboshan, and H. R. Nazif, "Heat transfer enhancement and entropy generation analysis of Al_2O_3-water

nanofluid in an alternating oval cross-section tube using two-phase mixture model under turbulent flow", *Heat and Mass Transfer*, Vol. 54, No. 10, pp. 3171-3183, (2018).

[7] H. Najafi Khaboshan, and H. R. Nazif, "Numerical analysis on convective turbulent air in an alternating elliptical tube", *Modares Mechanical Engineering*, Vol. 16, No. 13, pp. 5-8, (2016).

[8] F. M. White, *Viscous fluid flow*, 2nd ed., McGraw-Hill, New York, (1991).

[9] B. E. Launder, and D. B. Spalding, *Lectures in mathematical models of turbulence*, Academic Press, London, (1972).

[10] H. Najafi Khaboshan, and H. R. Nazif, "The effect of multi-longitudinal vortex generation on turbulent convective heat transfer within alternating elliptical axis tubes with various alternative angles", *Case Studies in Thermal Engineering*, Vol. 12, pp. 237-247, (2018).

[11] M. Wolfshtein, "The velocity and temperature distribution in one-dimensional flow with turbulence augmentation and pressure gradient", *International Journal of Heat and Mass Transfer*, Vol. 12, No. 3, pp. 301-318, (1969).

[12] Z. Y. Guo, "A brief introduction to a novel heat-transfer enhancement heat exchanger", internal report, Department of EMEMKLEHTEC, Tsinghua University, Beijing, China, (2003).

[13] J. P. Van Doormaal, and G. D. Raithby, "Enhancements of the SIMPLE method for predicting incompressible fluid flows", *Numerical Heat Transfer*, Vol. 7, No. 2, pp. 147-163, (1984).

[14] A. J. Chorin, "Numerical solution of the Navier-Stokes equations", *Mathematics of Computation*, Vol. 22, No. 104, pp. 745-762, (1968).

[15] H. K. Versteeg, and W. Malalasekera, *An introduction to computational fluid dynamics: the finite volume method*, 2nd ed., Pearson Education, England, (2007).

[16] D. G. Holmes, and S. D. Connell, "Solution of the 2D Navier-Stokes equations on unstructured adaptive grids". *Proc. of 9th Computational Fluid Dynamics Conference*, p. 1932, (1989).

[17] R. D. Rausch, J. T. Batina, and H. T. Y. Yang, "Spatial adaption procedures on unstructured meshes for accurate unsteady aerodynamic flow computation". *Proc. of 32nd Structures, Structural Dynamics, and Materials Conference*, p. 1106, (1991).

[18] R. F. Warming, and R. M. Beam, "Upwind second-order difference schemes and applications in aerodynamic flows", *AIAA Journal*, Vol. 14, No. 9, pp. 1241-1249, (1976).

[19] B. E. Launder, and D. B. Spalding, "The numerical computation of turbulent flows", *Computer Methods in Applied Mechanics and Engineering*, Vol. 3, No. 2, pp. 269-289, (1974).

[20] W.-L. Chen, Z. Guo, and C. o.-K. Chen, "A numerical study on the flow over a novel tube for heat-transfer enhancement with a linear Eddy-viscosity model", *International Journal of Heat and Mass Transfer*, Vol. 47, No. 14, pp. 3431-3439, (2004).

[21] B. S. Petukhov, T. F. Irvine, and J. P. Hartnett, *Advances in heat transfer*, Academic Press, New York, (1970).

[22] V. Gnielinski, "New equations for heat and mass-transfer in turbulent pipe and channel flow", *International Chemical Engineering*, Vol. 16, No. 2, pp. 359-368, (1976).

[23] T. L. Bergman, A. S. Lavine, F. P. Incropera, and D. P. Dewitt, *Fundamentals of heat and mass transfer*, 7th ed., John Wiley & Sons, New Jersey, p. 545, (2011).

[24] R. L. Webb, and N.-H. Kim, *Principles of enhanced heat transfer*, Taylor Francis, New York, (1994).

How to cite this paper:

Hasan Najafi Khaboshan and Hamid Reza Nazif, "Numerical analysis of heat transfer enhancement and flow structure of alternating oval tubes by considering different alternate angles under turbulent flow", *Journal of Computational and Applied Research in Mechanical Engineering,* Vol. 9, No. 2, pp. 211-223, (2020).

DOI: 10.22061/jcarme.2018.2974.1311

URL: http://jcarme.sru.ac.ir/?_action=showPDF&article=903